Appl Phys A (2010) 99: 323–331
DOI 10.1007/s00339-009-5535-1

Applied Physics A
Materials Science & Processing

Enhanced polarization and magnetoelectric response in $Tb_{1-x}Ho_xMnO_3$

C.L. Lu · S. Dong · K.F. Wang · J.-M. Liu

Received: 30 September 2009 / Accepted: 14 December 2009 / Published online: 29 December 2009

Abstract A series of manganites $Tb_{1-x}Ho_xMnO_3$ ($0 \leq x \leq 0.6$) with orthorhombic structure are synthesized and detailed investigations on their multiferroicity are performed. Successive magnetic transitions upon temperature variation are evidenced for all the samples, and both the Mn^{3+}spiral spin ordering and rare-earth spin ordering are suppressed with increasing x. A significant enhancement of both the polarization and magnetoelectric response within $0.2 < x < 0.4$ is observed, which may probably result from the shortening of the spiral-spin-ordering period, due to the competition between the spiral spin order and E-type antiferromagnetic order. This argument is supported by further theoretical calculations based on the two e_g-orbital double-exchange model.

1 Introduction

Multiferroic manganites $RMnO_3$ (R = Tb, Dy etc.) with orthorhombic structure have been intensively investigated since the discovery of the gigantic magnetoelectric (ME) effect in $TbMnO_3$ [1–5]. They show simultaneous reversal of ferroelectric (FE) polarization (P) and magnetization (M) upon sweeping magnetic field H [6]. This cross-coupling between M and P is of fundamental interest and provides an additional degree of freedom, not only in designing memory elements. Investigations [7–14] revealed that the noncollinear spiral spin order is essential to the onset of polarization. A possible microscopic mechanism for this spiral-spin driven ferroelectricity is the inverse Dzialoshinski–Moriya (DM) interaction or spin current scenario [8, 15, 16], in which two nearest-neighbor noncollinear spins displace the intervening oxygen through the electron-lattice interaction. Accordingly, the correlation between P and two noncollinearly coupled spins is given by $\boldsymbol{P} \propto \boldsymbol{e}_{ij} \times (\boldsymbol{S}_i \times \boldsymbol{S}_j)$, where $\boldsymbol{e}_{ij}$ denotes the unit vector connecting the two spins $\boldsymbol{S}_i$ and $\boldsymbol{S}_j$.

However, when the A-site ion Tb^{3+} (Dy^{3+}) is replaced by Ho^{3+}, which has smaller ionic radius [17], the Mn spins form a collinear E-type antiferromagnetic (E-AFM) order with commensurate wavevector [18], and it was predicted [19] that the FE order can exist in this E-AFM structure, caused by a balance between double-exchange (DE) electron-hopping and elastic energy, and that the quantum-mechanical effects of electron-orbital polarization is vital to ferroelectricity generation [20]. These predictions were evidenced in $HoMnO_3$ recently [21, 22]. Here, one notes that the origin of ferroelectricity in the E-AFM structure is different from that in spiral-spin-order (SSO) systems, and a first-order phase transition between the SSO and E-AFM order has been predicted [11]. On the other hand, $DyMnO_3$ [5], which is located between $TbMnO_3$ and $HoMnO_3$, exhibits the largest electrical polarization and ME effect, larger than its neighbors. Along this line, it would be of interest to reveal what the intermediate state and the associated physical

C.L. Lu · K.F. Wang · J.-M. Liu (✉)
Laboratory of Solid State Microstructures, Nanjing University, Nanjing 210093, China
e-mail: liujm@nju.edu.cn

S. Dong
Department of Physics, Southeast University, Nanjing 210008, China

K.F. Wang · J.-M. Liu
School of Physics, South China Normal University, Guangzhou 510006, China

J.-M. Liu
International Center for Materials Physics, Chinese Academy of Science, Shenyang 110016, China

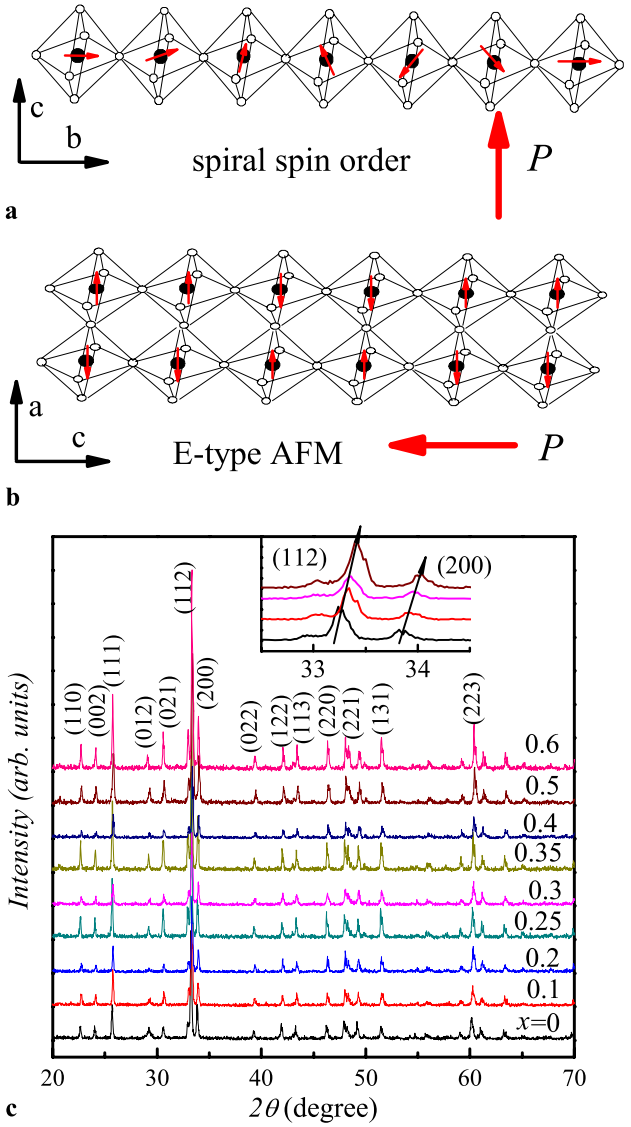

Fig. 1 Schematic drawing of the crystallographic and spin structures of manganites $TbMnO_3$ and $HoMnO_3$: (**a**) spiral spin order for $TbMnO_3$, and (**b**) E-type AFM order for $HoMnO_3$. The *open circles* present the oxygen ions, and the *black dots* present the Mn^{3+}. For clarity, only the octahedron units are given. (**c**) Room temperature X-ray diffraction patterns of $Tb_{1-x}Ho_xMnO_3$ ($0 \le x \le 0.6$). The *inset* shows the diffraction peaks of (112) and (200) planes for samples with $x = 0$, 0.1, 0.3, 0.5 from bottom to up, respectively

properties are as the A-site cation changes from Tb to Ho. Schematic drawings of crystallographic and spin structures of the $TbMnO_3$ manganites with SSO and $HoMnO_3$ with E-AFM order are shown in Figs. 1(a) and (b), respectively.

In this paper, we address this issue by focusing on $TbMnO_3$ as the prototype sample via successive doping of Tb^{3+} with Ho^{3+}, intending to investigate the evolving of P and ME effect in $Tb_{1-x}Ho_xMnO_3$. Subsequently, we perform a series of measurements on the multiferroicity. We will reveal the enhanced P and ME coupling between P and M, which is argued to be due to the shortening of the spiral-spin-ordering period mediated by the E-AFM order. This Ho^{3+}-substitution effect is further studied by a theoretical calculation, which reveals consistency with our experimental results.

2 Experimental procedure

Polycrystalline $Tb_{1-x}Ho_xMnO_3$ ($0 \le x \le 0.6$) samples were prepared by a conventional solid-state reaction. The highly purified powders of oxides were mixed in stoichiometric ratios, ground, and then fired at 1200°C for 24 hours (h) in an oxygen flow. The resultant powders were reground and pelletized and then sintered at 1350°C for 24 hours in an oxygen flow with intermediate grindings. X-ray diffraction (XRD) with Cu $K\alpha$ radiation was performed on these samples at room temperature (T). The magnetic and specific-heat measurements using a superconducting quantum interferometer device (SQUID) and physical properties measurement system (PPMS), both from Quantum Design Ltd., were performed to probe the magnetization and spin orders.

For measuring dielectric constant ε and polarization P, gold pastes were used as electrodes, and varying T and H were provided by PPMS. We measured ε using the HP4294 impedance analyzer, while P as a function of T was evaluated from the pyroelectric current measured by a Keithley 6514A electrometer after cooling the samples under selected electric fields, and detailed discussion on the procedure of this measurement can be found in an earlier report [21–24]. We will also address several issues of this technique related to the ferroelectricity measurement.

3 Results and discussion

3.1 Multiferroic behaviors

We identify the crystallinity and structure of the as-prepared samples. The XRD patterns of all the samples are presented in Fig. 1(c). All the reflections suggest that our samples are polycrystalline and can be indexed by a single orthorhombic structure of space group *Pbnm*. The relative intensity of these reflections shows one-to-one correspondence with the standard JPCD database, indicating that the microstructure is not textured. A continuous shifting of these reflections towards the high angle side with increasing x, as more clearly identified in the inset, indicates the weak lattice contraction with increasing x. This variation is reasonable because of slightly smaller Ho^{3+} than Tb^{3+}.

We pay more attention to the magnetic ordering and corresponding P-generation. As an example, we present in Figs. 2(a) and (b) the measured M, specific heat divided

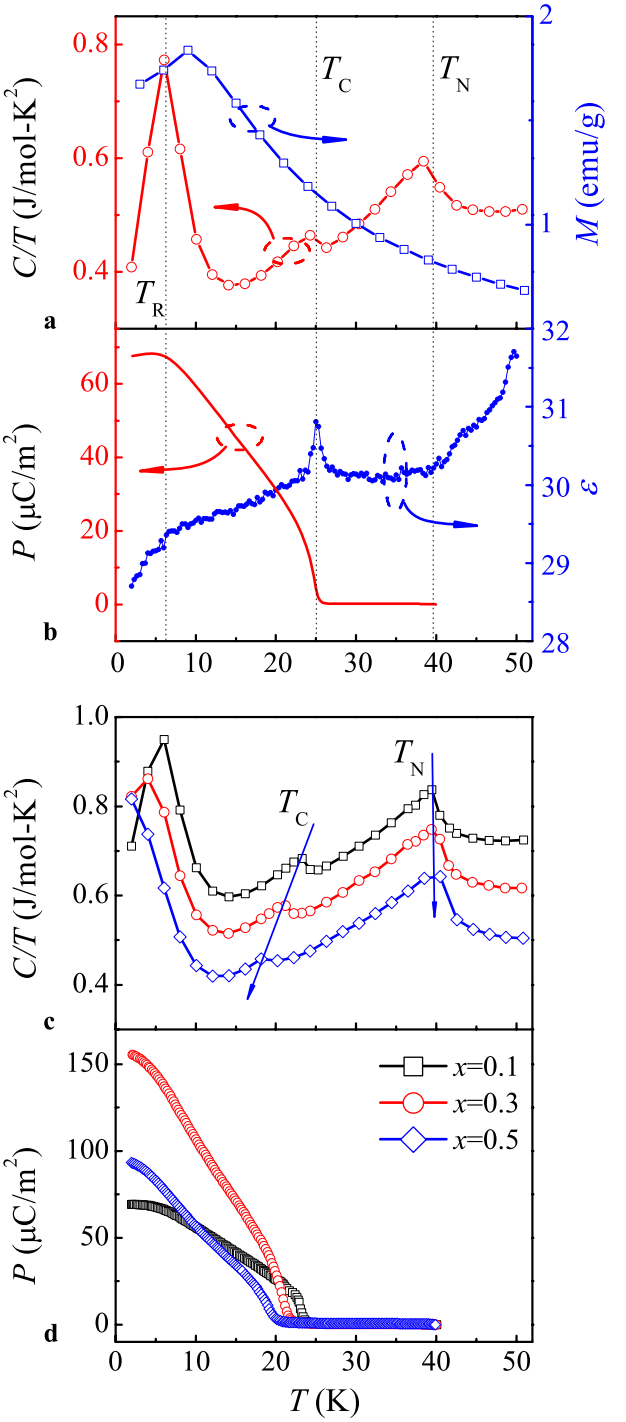

Fig. 2 Temperature profiles of (**a**) specific heat divided by temperature C/T and magnetization, and (**b**) dielectric constant ε and electric polarization P for sample $TbMnO_3$. (**c**) Measured C/T and (**d**) P as a function of T for samples $x = 0.1$, 0.3, 0.5, respectively. The *vertical dot lines* in (**a**) and (**b**) mark T_N, T_C, T_R, respectively. The poling field is 3 kV/cm

by T (C/T), ε, and P as a function of T for the sample with $x = 0$ ($TbMnO_3$). It is clearly shown that the measured M is small and shows no anomaly over the whole T-range covered in the present experiments, indicating no ferromagnetic spin correlation. The reason lies in the fact that all possible spin orders are AFM-type [25]. We then consult the C/T data, which are sensitive to such types of ordering. The anomaly at $T = T_N = 40$ K corresponds to the onset of a collinear sinusoidal spin ordering with an incommensurate wavevector, where $\varepsilon(T)$ also exhibits a distinct kink. A second anomaly at $T = T_C = 25$ K develops a noncollinear spiral spin order with a T-independent wavevector, at which a nonzero P ensues and which is accompanied with a sharp peak in $\varepsilon(T)$. Upon further cooling down to $T = 6$ K, a third anomaly of C/T associated with the long-range ordering of Tb^{3+} moments can be identified. The successive phase transitions in terms of C/T together with the magnetization and dielectric response (shown below) are in agreement with earlier reports [1–5], and the microstructural evolution associated with the phase transitions is confirmed. These one-to-one correspondences between the Mn^{3+} spin orders and polarization generation do indicate a strong cross-coupling between the magnetic and ferroelectric orders.

Now we address the evolution of the measured data with varying x. Three typical sets of data are shown in Figs. 2(c) and (d), respectively. It seems that T_N is independent of x, but T_C and T_R show continuous down-shifting as x increases from 0 to 0.5. Considering the facts that T_N for $TbMnO_3$ and $HoMnO_3$ is ~41 K and not much additional lattice distortion associated with the doping is generated since the Tb^{3+} radius (~1.095 Å) is close to Ho^{3+} radius (~1.072 Å) [17], one expects no remarkable change of T_N upon the doping, a reasonable argument, consistent with measured results. However, because T_C is the onset point of the spiral spin order, Ho^{3+}-doping at the Tb^{3+}-site indicates the suppression of the spiral spin ordering down to a lower T, characterized by the downshift of this onset point. It is also identified that T_R disappears at $x \sim 0.5$, revealing no more Tb^{3+} long-range spin order to be possible at half-doping and higher. What is most interesting here is the x-dependence of the measured P at low T. It is seen that the value of P for the sample with $x = 0.3$ is almost double that for $TbMnO_3$, indicating significant enhancement of P upon such doping. Surely, for over-high doping, e.g. $x = 0.5$ here, we observe a downshift of P back to a value similar to $HoMnO_3$ [21, 22].

To obtain a more comprehensive picture of the doping effect, the measured P as a function of poling field E at $T = 2$ K for selected samples are evaluated, and the data for samples $x = 0$ and 0.3 are shown in Fig. 3(a). It is revealed that the measured P first grows with increasing E and then tends to be saturated under high E. The present data show that the remnant polarization P_r associated with the saturated polarization can be roughly obtained at $E > 5$ kV/cm. Clearly, the $x = 0.3$ sample possesses a much larger P_r than the sample with $x = 0$, indicating significantly enhanced ferroelectricity with respect to the sample with $x = 0.0$.

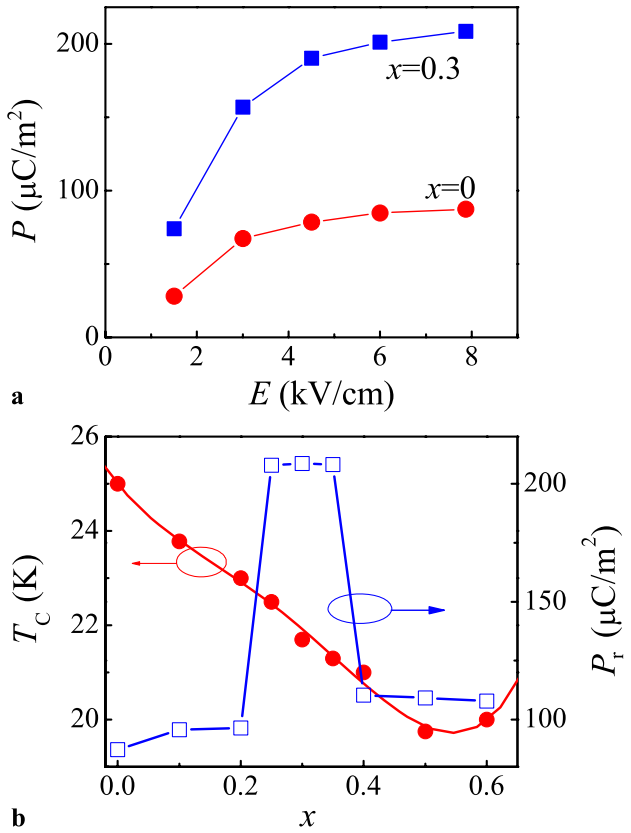

Fig. 3 (**a**) E-dependence of P at $T = 2$ K for samples $x = 0$ and 0.3. (**b**) The measured T_C and P_r at $E = 8$ kV/cm of $Tb_{1-x}Ho_xMnO_3$ ($0 \le x \le 0.6$) as a function of x. The *red dots* represent the paraelectric-ferroelectric transition point T_C, and the *blue squares* represent the measured P_r at $T = 2$ K. Both the *red* and *blue lines* are guide for the eyes

In Fig. 3(b), the measured $T_C(x)$ and $P_r(x)$ at $E = 8$ kV/cm with more data are presented. We observe a roughly linear suppression of T_C with x until $x = 0.5$ at which T_C reaches its minimal value at ~ 19.5K, followed by a slight return at $x = 0.6$ beyond which the sample synthesis by conventional route becomes tough. Such a suppression possibly can be understood by the doping induced E-AFM order (in $HoMnO_3$) in competition with the SSO in $TbMnO_3$. This fact may allow one to expect a smooth suppression of P_r in terms of the onset point (T_C) and magnitude, upon the doping. Nevertheless, the multiferroic physics associated with the Ho^{3+}-doping seems more complicated. The measured $P_r(x)$ at $T = 2$ K exhibits a very unusual behavior, as shown in Fig. 3(b) too. Over the range $0 < x < 0.6$, $P_r(x)$ does not decay in synchronization with $T_C(x)$. Instead, it does not change much with x up to ~ 0.2 at which $P_r(x)$ exhibits a jump from 87 μC/m^2 to $\sim$210 μC/m^2, a significant enhancement. This enhancement is maintained until $x > 0.4$ at which $P_r(x)$ again falls down to $\sim$110 μC/m^2 and then decays slowly with x.

3.2 Magnetoelectric response

In order to get a deeper understanding of this doping effect, we turn to the ME effect. The measured $P(T)$ at several selected H for selected samples are shown in Fig. 4. For the sample with $x = 0$, T_C is independent of H, consistent with earlier report [1], a small increase of P below T_C with increasing H is identified, associated with the multiple domains. Similar increase in P caused by the magnetic field can also be observed in the sample with $x = 0.1$. For increased doping level x, P can be significantly reduced by H, and the largest ME response (defined as $\text{ME} = (P(0) - P(H))/P(0)$) is evidenced for the sample with $x = 0.3$ and reaches about $\sim$86% at $H = 9$ T at low T. It should be addressed that such a large ME response cannot be obtained at $x < 0.2$ and $x > 0.4$, indicating the one-to-one correspondence between the P-enhancement and the ME response.

On the other hand, for the sample with $x = 0.3$, the dielectric susceptibility also shows an unusual response to the magnetic field, and ε evolves with T in a different way when $x > 0.3$, as shown in Fig. 5. Considering the fact that the E-AFM order ($HoMnO_3$) contributes a lot to the dielectric constant, but a spiral one ($TbMnO_3$) does not [21, 22], the present results suggest that the E-AFM order becomes important in the samples where $x > 0.3$, and also in the sample with $x = 0.3$ under magnetic field, in agreement with the above results.

3.3 Discussion

An understanding of the physics underlying the Ho^{3+}-doping effects is challenging. For the unusual enhancement of $P_r(x)$ over $0.2 < x < 0.4$, one may argue: (1) the large enhancement of P_r can be simply ascribed to neither the contribution of the spiral spin order (favored in $TbMnO_3$) nor the E-AFM orders (favored in $HoMnO_3$), since the P-value of either polycrystalline $TbMnO_3$ ($\sim$87 μC/m^2) or orthorhombic $HoMnO_3$ ($\sim$90 μC/m^2) is much smaller than $\sim$210 μC/m^2; (2) if the Ho^{3+}-doping causes simply the solid-solution effect that the magnetic configuration is composed of spiral spin order as in $TbMnO_3$ and E-AFM order as in $HoMnO_3$, P is expected to be within [87 μC/m^2, 90 μC/m^2]. Referring to the extremely large electrical polarization and ME effect in the intermediate material $DyMnO_3$ [5], which has a shorter period of the SSO than $TbMnO_3$, one possible explanation is that the period of the SSO within samples $0.2 < x < 0.4$ comparable with that in $DyMnO_3$, caused by the competition between the SSO and E-AFM order, since the two essentially different phases are neighboring to each other in the phase diagram. Indeed, a first-order transition was predicted theoretically between the two essentially different spin orders, and it is reasonable to

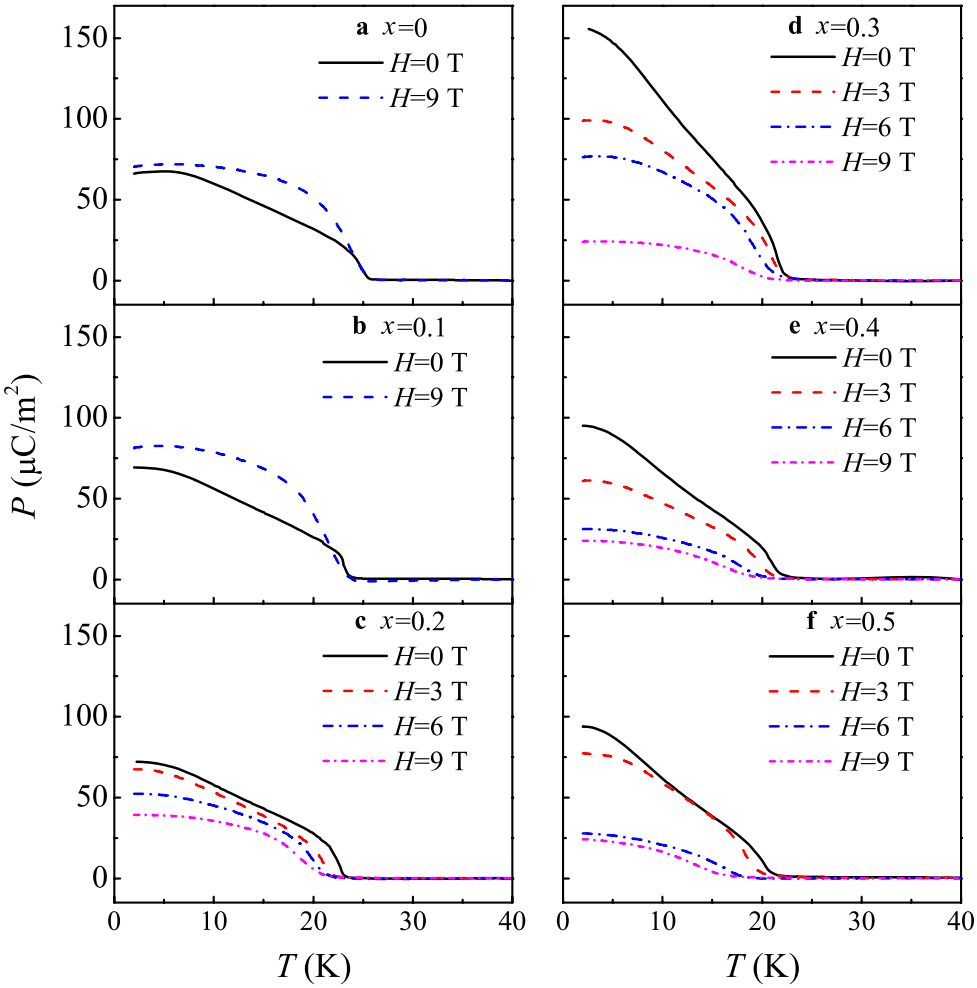

Fig. 4 Magnetic field modulation of polarization as a function of T for samples with $x = 0, 0.1, 0.2, 0.3, 0.4, 0.5$, respectively. The poling field is 3 kV/cm

anticipate such a two-phase competing in the energy landscape [11]. Surely, we do not have sufficient evidence for such a competition, which appeals to an additional experimental exploration, using e.g. neutron scattering techniques.

On the other hand, for the large ME response in the sample with $x = 0.3$, we note that in $TbMnO_3$, an applied H drives the rotation of the spiral plane from the bc plane to the ab plane, and the corresponding P is switched from the c-axis to the a-axis [5]. This spiral plane rotation will not induce significant variation of P in a polycrystalline sample, as shown in Fig. 4(a) for the sample with $x = 0$. For E-AFM order induced ferroelectricity, an external H suppresses the E-AFM orders rather than enhancing it, and a large ME response has been evidenced [21, 22]. Therefore, one may correlate the large ME effects in $Tb_{1-x}Ho_xMnO_3$ with the suppression of E-AFM order. If this would be true, one should expect a monotonous increase of the ME response with x and the maximum at $x = 1$ ($HoMnO_3$). However, our results confirm that the ME response does not monotonically increase with x but reaches a maximum around $x \sim 0.3$, coincident with the $P_r(x)$-dependence. Also the ground state of the sample with $x = 0.3$ cannot be the E-AFM order, since its physical property is rather different from $HoMnO_3$. Therefore, the large ME response in our samples, for example for the sample where $x = 0.3$, possibly can be associated with the short period of SSO as in $DyMnO_3$ [5]. This supposition is consisted with the origination of the electric polarization. Nevertheless, it should be mentioned that a clear understanding of the Ho^{3+}-doping effects revealed here still needs theoretical explanation, to be given below.

4 Theoretical study

To further understand our experimental results illustrated above, we start from the two-orbital double-exchange (DE) model and perform extensive simulations on the enhancement of P and ME effect. This DE model has been extensively employed for understanding the physics in manganites, as done in [11] for example and successfully reproducing the electronic phase diagram of $RMnO_3$ by tuning the nearest-neighbor (NN) superexchange (SE) factor, J_{AF}, and the next-nearest-neighbor (NNN) SE factor along the b-axis, J_{2b}.

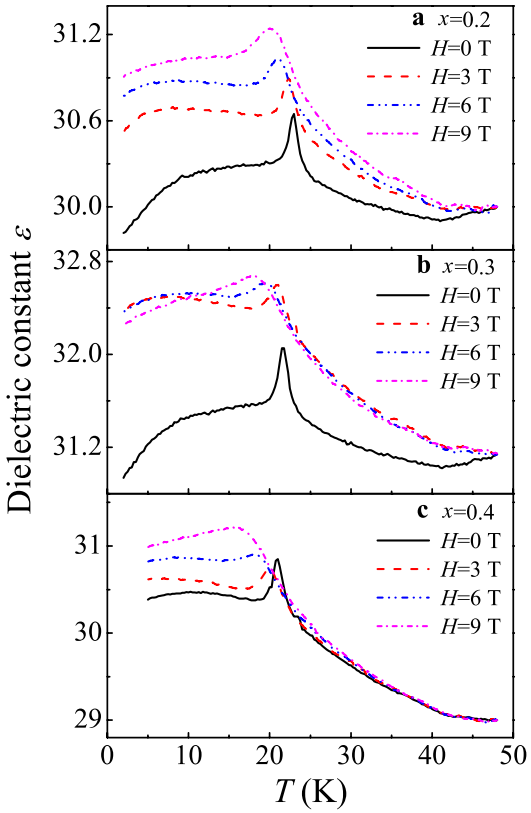

Fig. 5 Magnetic field modulation of dielectric constant as a function of T for the sample with $x = 0.2, 0.3, 0.4$, respectively

We consider the orthorhombic lattice distortion, as identified for the present system, where the NNN SE factor along the a-axis, which is weaker than J_{2b}, is neglected for simplification [11]. By tuning the combination (J_{AF}, J_{2b}), the ground state can change from the A-type AFM (A-AFM) state to the SSO, and eventually to the E-AFM state. For example, given a properly chosen Jahn–Teller (JT) distortion, $\lambda|Q_2| = 1.5$, a choice of $(J_{AF} = 0.087,\ J_{2b} = 0.008)$ allows for a SSO state with $k = 1/6$ (k is the wave number along the pseudocubic [100] and [010] axes), while a choice of $(J_{AF} = 0.1,\ J_{2b} = 0.01)$ favors an E-AFM phase. Note that these parameters are normalized by the DE hopping energy $t_0 \sim 0.2$–0.3 eV and the same applies hereafter. More details of the model description and computations can be found in [11].

We start from a 12×12 lattice with periodic boundary conditions [11]. For a realistic and infinite $R\mathrm{MnO_3}$ system of SSO state, e.g. $\mathrm{Tb_{1-x}Dy_xMnO_3}$, the wave number k should change continuously with varying x. However, because of the finite lattice here only a discrete set of wave numbers accommodating the SSO state is allowed. In other words, the wave number k for the possible SSO phase is discrete, i.e. 1/12, 1/6, 1/4, 1/3, 1/2. Surely, a larger lattice size can improve the precision of the number k associated with the SSO phase, however, the CPU time for the efficient computation will also increase extremely fast with increasing lattice size for the DE model. Although the classical spin models can handle larger lattices for the SSO phase [26], it is under debate whether the E-AFM order can exist in these models. Therefore, in the present work, we fix our simulation in the 12×12 lattice.

To take into account the doping effect at the A-site for $\mathrm{Tb_{1-x}Ho_xMnO_3}$, we consult the A-site disorder scenario extensively investigated by most previous theoretical studies on the A-site doped manganites. We treat the A-site disordering effect due to the Ho-doping as a random on-site potential field onto the NN/NNN superexchange interactions. Such a potential field originates from the alloy-mixed cations with different valences. For $\mathrm{Tb_{1-x}Ho_xMnO_3}$, both Tb and Ho ions take $+3$ charges and the A-site disorder is mainly from the cation size difference, which affects the Mn–O–Mn bond-angles and thus the exchange interactions. To mimic this effect, the random field is only applied onto the SE terms, while the DE and JT distortion terms are assumed to be independent of the random field for simplification consideration.

In our simulation, a random distribution of the A-site cations (Tb, Ho) is generated on a two-layer 12×12, where the two layers are the two NN AO layers of $\mathrm{MnO_2}$ plane. Then the NN/NNN SE factors are calculated based on the A-site cation distribution. Each factor J_{AF} is determined by its four NN A-site cations, while each J_{2b} is determined by its two NN A-site cations, as by

$$\begin{aligned} J_{AFi} &= \left(n_i^{\mathrm{Tb}} J_{AF}^{\mathrm{Tb}} + n_i^{\mathrm{Ho}} J_{AF}^{\mathrm{Ho}}\right)/4, \\ J_{2bj} &= \left(n_j^{\mathrm{Tb}} J_{AF}^{\mathrm{Tb}} + n_j^{\mathrm{Ho}} J_{AF}^{\mathrm{Ho}}\right)/2, \end{aligned} \tag{1}$$

where n_i denote the number of the NN A-site cations (Tb or Ho) surrounding bond i.

In $\mathrm{TbMnO_3}$, the SSO state has a wave number $k \sim 0.14$, corresponding to $(J_{AF} = 0.086,\ J_{2b} = 0.006)$ in our model if the JT distortion $\lambda|Q_2| = 1.5$ is fixed. However, for this 12×12 lattice, a choice of such a set of parameters $(J_{AF} = 0.086,\ J_{2b} = 0.006,\ \lambda|Q_2| = 1.5)$ will give rise to the SSO phase of wave number $k = 1/6$ instead of $k \sim 0.14$, due to the aforementioned finite size limit. Furthermore, it is noted that any SSO phase with $k \geq 0.24$ is unfavored, since its energy is always higher than that of the E-AFM phase. Therefore, in our simulation, we begin from $k = 1/12$ and investigate the evolution of k as a function of x. For realizing this, we choose $(J_{AF}^{\mathrm{Tb}},\ J_{2b}^{\mathrm{Tb}}) = (0.085, 0.005)$ and $\lambda|Q_2| = 1.5$ in the following simulation, corresponding to a SSO phase of $k = 0.12$ in the infinite lattice and $k = 1/12$ in the present 12×12 lattice. Meanwhile, $(J_{AF}^{\mathrm{Ho}},\ J_{2b}^{\mathrm{Ho}}) = (0.1, 0.01)$ is fixed too, which can stabilize an E-AFM order.

Initialized with a random spin lattice, the simulation using the Monte Carlo (MC) method is performed at $T = 0.002$ (∼5–7 K), which is low enough to approach the

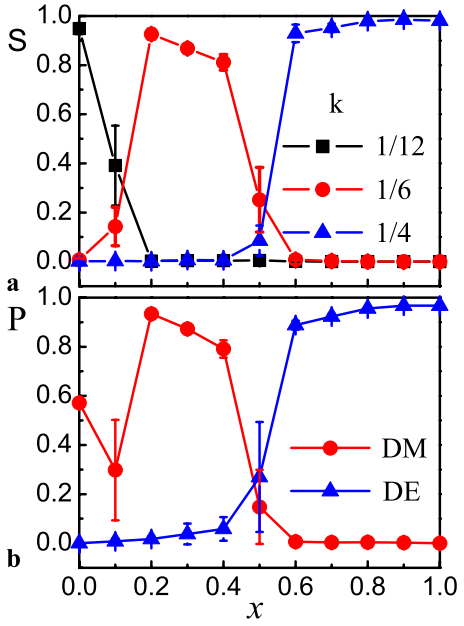

Fig. 6 Ho^{3+}-doping level x-dependence of (**a**) spin structure factors and (**b**) ferroelectric polarizations originated from the DM interaction and DE process. The phase coexistence (separation) between the E-AFM phase and SSO phase occurs at $x = 0.5$, indicated by the coexisting spin orders and large fluctuations (*error bars*). In (**a**), $k = 1/12$ and $k = 1/6$ are for the SSO phases, while $k = 1/4$ is for the E-AFM phase. Both polarizations are normalized to their saturation values ($k = 1/6$ and E-AFM) respectively. Since the real ratio between these two polarizations is unclear, the absolute value of the total polarization is unavailable in our simulation

ground state. After the MC sequence for 12000 MC steps, a zero-T optimization is used to confirm this prediction of the ground state. For each concentration x, three independent distributions of the random field have been tested and the data are averaged. To reveal the evolution of spin order against doping level x, the spin structure factor (SSF) is calculated. In addition, the ferroelectricity based on the DM mechanism ($\sim \sum_{\langle ij \rangle} e_{ij} \times (S_i \times S_j)$) and DE mechanism[1] are evaluated respectively.

The calculated SSF as a function of wave number k, $S(k, k)$, at various x, are shown in Fig. 6(a). With increasing x, the SSO phase with $k = 1/12$ is rapidly suppressed while that with $k = 1/6$ becomes the dominant one. Interestingly, at $x = 0.1$, the coexistence of components $k = 1/12$ and $k = 1/6$ as well as their tremendous fluctuations likely suggests the possibility of the two-phase coexistence. Nevertheless, this coexistence is caused by the finite size limit, which does not allow a continuous modulation of k from $1/12$ to $k = 1/6$, while in realistic materials this transition should be of the second order. Meanwhile, the ferroelectric polarization P induced by the DM interaction is enhanced in the range of $x = 0.2$ to 0.4, as shown in Fig. 6(b). At $x \sim 0.5$, the coexistence of the E-AFM ($k = 1/4$) and the SSO ($k = 1/6$) ensues, as characterized by the SSF data and polarization data. Beyond $x = 0.5$, the E-AFM spin order becomes the dominant one and the ferroelectricity is mainly driven by the DE mechanism. These calculations seem well consistent with the experimental data, while it should be pointed out that it does not make quantitative sense to directly compare the doping level x in the calculation with the experimental one since we have the finite size limit.

In Fig. 7 are presented several examples of a snapshot of the spin pattern, which also confirm the phase transitions with increasing x. For Figs. 7(a), (b), and (d), the spin order can be described by the phases with almost pure $k = 1/12$ ($x = 0$), $k = 1/6$ ($x = 0.2$) and E-AFM ($x = 1$), respectively. In particular, the E-AFM zigzag segments and SSO clusters coexist in Fig. 7(c) at $x = 0.5$.

In short, the two-orbital DE model has been studied to mimic the Ho-doping effects in $Tb_{1-x}Ho_xMnO_3$. Although limited by the finite size effects, a qualitative agreement between the model simulation and experimental measurements remains robust. With increasing x, the ferroelectric polarization P is enhanced by the increasing spiral wave number k (shortening of spiral period). This is in agreement with our argument based on the experimental results. In addition, an interesting feature is predicted by our calculation: that there is possible multiferroic phase coexistence (PS) ensuing near the phase boundary between the SSO phase and E-AFM phase. In this sense, what the intrinsic correlation is between this multiferroic phase coexistence and the large ME response within samples $0.2 < x < 0.4$ remains an interesting issue [27]. But this issue needs more extensive investigation using advanced and specific techniques.

5 Conclusion

In conclusion, we have performed experimental and theoretical investigations on the magnetism, specific heat, electric polarization, and dielectric susceptibility in the manganite multiferroics $Tb_{1-x}Ho_xMnO_3$. The appropriate A-site doping using Ho^{3+} to replace Tb^{3+} simultaneously enhances the electric polarization and magnetoelectric response significantly over the doping range from $x = 0.2$ to $x = 0.4$. The enhancement of both the P and ME response may probably be ascribed to the shortening of the period of SSO mediated by the coexisting E-AFM order, due to the competition between the SSO and E-AFM order. Our calculation shows good consistency with the experimental results.

[1] In our simulation, a phenomenological equation ($\sim \boldsymbol{r}_{ij}\sqrt{1 + \boldsymbol{S}_i \cdot \boldsymbol{S}_j}$) is used to evaluate the ferroelectric polarization P driven by the DE process, as in the E-AFM phase. Here the term $\sqrt{1 + \boldsymbol{S}_i \cdot \boldsymbol{S}_j}$ is the NN DE intensity in the classical approximation, and $\boldsymbol{r}_{ij}$ denotes the oxygen displacement vector (due to the $GdFeO_3$ distortion) from the midpoint of the NN Mn bond, which is $+-+-$ staggered along the pseudocubic [100] and [010] axes. More information about the DE driven ferroelectricity can be found in [19, 20].

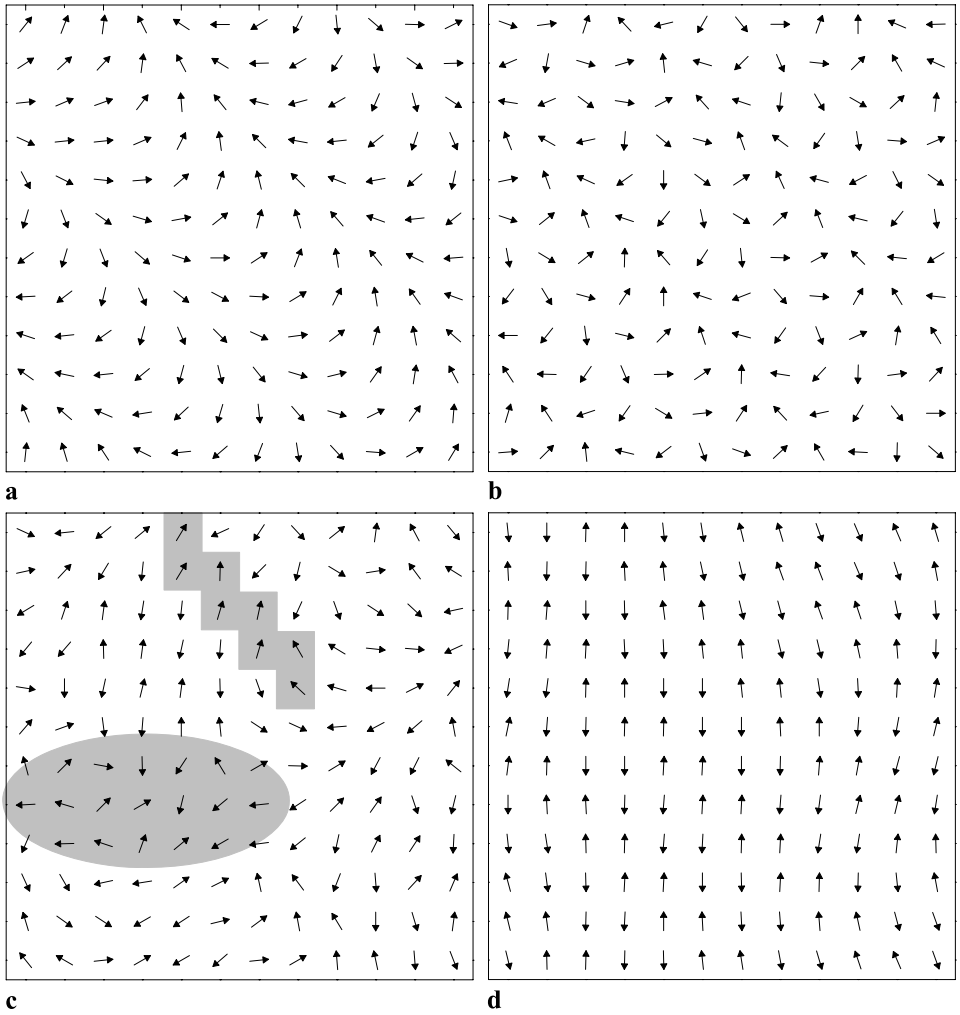

Fig. 7 Spin patterns of Mn cations obtained after the MC simulation and optimization. (**a**–**d**) are for $x = 0$, 0.2, 0.5, 1.0, respectively. For (**a**), (**b**), and (**d**), the spin orders are almost pure $k = 1/12$ and $k = 1/6$ spiral-spin patterns, as well as E-AFM pattern, respectively. The coexisting SSO and E-AFM segments are highlighted in (**c**)

Acknowledgements S.D. thanks E. Dagotto, S.-W. Cheong, T. Kimura, and N. Nagaosa for helpful discussions. This work was supported by the Natural Science Foundation of China (10874075, 50832002), the National Key Projects for Basic Research of China (2009CB623303, 2009CB929501, 2006CB921802), and the Natural Science Foundation of China in Jiangsu (BK2008024).

References

1. T. Kimura, T. Goto, H. Shintani, K. Ishizaka, T. Arima, Y. Tokura, Nature **426**, 55 (2003)
2. K.F. Wang, J.-M. Liu, Z.F. Ren, Adv. Phys. **58**, 321 (2009)
3. S.-W. Cheong, M. Mostovoy, Nat. Matter **6**, 13 (2007)
4. J.-H. Lee, P. Murugavel, D. Lee, T.W. Noh, Y. Jo, M.-H. Jung, K.H. Jang, J.-G. Park, Appl. Phys. Lett. **90**, 012903 (2007)
5. T. Kimura, G. Lawes, T. Goto, Y. Tokura, A.P. Ramirez, Phys. Rev. B **71**, 224425 (2005)
6. N. Abe, K. Taniguchi, S. Ohtani, T. Takenobu, Y. Iwasa, T. Arima, Phys. Rev. Lett. **99**, 227206 (2007)
7. M. Mostovoy, Phys. Rev. Lett. **96**, 067601 (2006)
8. H. Katsura, N. Nagaosa, A.V. Balatsky, Phys. Rev. Lett. **95**, 057205 (2005)
9. H.J. Xiang, S.-H. Wei, M.-H. Whangbo, J.L.F.D. Silva, Phys. Rev. Lett. **101**, 037209 (2008)
10. A. Malashevich, D. Vanderbilt, Phys. Rev. Lett. **101**, 037210 (2008)
11. S. Dong, R. Yu, S. Yunoki, J.-M. Liu, E. Dagotto, Phys. Rev. B **78**, 155121 (2008)
12. M. Kenzelmann, A.B. Harris, S. Jonas, C. Broholm, J. Schefer, S.B. Kim, C.L. Zhang, S.-W. Cheong, O.P. Vajk, J.W. Lynn, Phys. Rev. Lett. **95**, 087206 (2005)
13. Y. Yamasaki, H. Sagayama, T. Goto, M. Matsuura, K. Hirota, T. Arima, Y. Tokura, Phys. Rev. Lett. **98**, 147204 (2007)
14. T. Kimura, Annu. Rev. Mater. Res. **37**, 387 (2007)
15. I.A. Sergienko, E. Dagotto, Phys. Rev. B **73**, 094434 (2006)
16. Q.C. Li, S. Dong, J.-M. Liu, Phys. Rev. B **77**, 054442 (2008)
17. R.D. Shannon, Acta Crystallogr., Sect. A, Cryst. Phys. Differ. Theor. Gen. Crystallogr. A **32**, 751 (1976)
18. A. Munoz, M.T. Casais, J.A. Alonso, M.J. Martinez-Lope, J.L. Martinez, M.T. Fernandez-Diaz, Inorg. Chem. **40**, 1020 (2001)
19. I.A. Sergienko, C. Şen, E. Dagotto, Phys. Rev. Lett. **97**, 227204 (2006)
20. S. Picozzi, K. Yamauchi, B. Sanyal, I.A. Sergienko, E. Dagotto, Phys. Rev. Lett. **99**, 227201 (2007)
21. B. Lorenz, Y.Q. Wang, C.W. Chu, Phys. Rev. B **76**, 104405 (2007)
22. B. Lorenz, Y.Q. Wang, Y.Y. Sun, C.W. Chu, Phys. Rev. B **70**, 212412 (2004)
23. C.L. Lu, J. Fan, H.M. Liu, K. Xia, K.F. Wang, P.W. Wang, Q.Y. He, D.P. Yu, J.-M. Liu, Appl. Phys. A **96**, 991 (2009)

24. N. Terada, T. Nakajima, S. Mitsuda, K. Kanedo, N. Metoki, Phys. Rev. B **78**, 104101 (2008)
25. C.C. Yang, M.K. Chung, W.-H. Li, T.S. Chan, R.S. Liu, Y.H. Lien, C.Y. Huang, Y.Y. Chan, Y.D. Yao, J.W. Lynn, Phys. Rev. B **74**, 094409 (2006)
26. M. Mochizuki, N. Furukawa, J. Phys. Soc. Jpn. **78**, 053704 (2009)
27. Y. Tokura, Rep. Prog. Phys. **69**, 797 (2006)